Nano Energy 33 (2017) 229–237

Contents lists available at ScienceDirect

Nano Energy

journal homepage: www.elsevier.com/locate/nanoen

Communication

Recycling $PM_{2.5}$ carbon nanoparticles generated by diesel vehicles for supercapacitors and oxygen reduction reaction

Guoyin Zhu[a], Tao Chen[a], Yi Hu[a], Lianbo Ma[a], Renpeng Chen[a], Hongling Lv[a], Yanrong Wang[a], Jia Liang[a], Xiaojie Li[a], Changzeng Yan[a], Hongfei Zhu[a], Haixia Liu[a], Zuoxiu Tie[a], Zhong Jin[a,*], Jie Liu[a,b,*]

[a] Key Laboratory of Mesoscopic Chemistry of MOE and Collaborative Innovation Center of Chemistry for Life Sciences, School of Chemistry and Chemical Engineering, Nanjing University, Nanjing, Jiangsu 210093, China
[b] Department of Chemistry, Duke University, Durham, NC 27708, USA

ARTICLE INFO

Keywords:
Particulate matter pollution
Diesel vehicle exhaust
Carbon nanoparticles
Supercapacitors
Oxygen reduction reaction

ABSTRACT

Particulate matter (PM) pollution has become a serious environmental problem, especially in developing countries, owing to its severe threat to human health. Particularly, airborne $PM_{2.5}$ (mean aerodynamic diameter ≤2.5 μm) particles are extremely harmful, because the tiny particles can enter human respiratory system and even penetrate into circulatory system. Herein, we propose an effective strategy to recycle $PM_{2.5}$ carbon nanoparticles generated by diesel vehicle engine for the applications of clean energy. After thermal treatment and purification, the $PM_{2.5}$ derived carbon nanoparticles show a diameter distribution between 25 and 40 nm, mesoporous characteristics (with an average pore size of ~3.3 nm), and homogeneous nitrogen incorporation (with N content of ~1.1 at%). The $PM_{2.5}$ derived N-doped mesoporous carbon nanoparticles were used as an advanced electrode material in supercapacitors, exhibiting excellent specific capacity and superb stability over long-term cycling. Moreover, the recycled $PM_{2.5}$ carbon nanoparticles show attractive electrocatalytic properties for oxygen reduction reaction, presenting high onset potential and good immunity to methanol crossover. We expect this research can provide inspiration for air pollution control and sustainable energy utilization.

1. Introduction

With the rapid growth of industry and economy, concomitant environmental problems are becoming more and more serious across developing countries, such as China and India [1,2]. In recent years, particulate matter (PM) pollution in the atmosphere has severely affected global air quality and public health [3–7]. According to the difference of particle size, PM can be divided into PM_{10} (aerodynamic diameter ≤10 μm) and $PM_{2.5}$ (aerodynamic diameter ≤2.5 μm) [8]. Notably, owing to the ultrafine diameter, $PM_{2.5}$ can easily enter human bronchi and lungs, and even can penetrate into blood circulation [9–11]. Moreover, with the rapidly increasing amount of vehicles and machines with internal combustion engines in urban and rural areas, the fumes from engine exhausts have already become one of the main sources of the $PM_{2.5}$ [12]. High concentration of $PM_{2.5}$ can trigger hazy and smog weather, which may lead to awful public health hazards, dust contaminations and traffic accidents.

Due to the above reasons, the prevention and control of $PM_{2.5}$ pollution has been extensively discussed recently [5,6,13,14]. Some novel methods have been developed to reduce $PM_{2.5}$ emissions or to reduce the harms caused by $PM_{2.5}$. For instances, Wang et al. designed a self-powered triboelectric filter for removing PMs from automobile exhaust fumes by triboelectrification effect [15]. Cui et al. prepared a transparent air filter via electrospinning of polymer nanofibers onto a metal-coated mesh for high-efficiency $PM_{2.5}$ capture [16]. However, the existing methods still cannot fully solve the pollution problems induced by suspended PMs.

The ultimate approach to solve environmental pollution and realize sustainable development is the utilization of clean energy sources (such as solar power, wind power and hydrogen energy) and high-efficiency energy conversion and storage devices (such as fuel cells [17–19], supercapacitors [20–22] and secondary batteries [23–25]). Fuel cells, as a clean energy production system, can directly produce electricity by oxygen reduction reaction (ORR) and the only byproducts are water and heat [26]. Meanwhile, as an emerging class of electrochemical energy storage devices, supercapacitors have received extensive attention over the past decade in view of many advantages, such as high power density, rapid charging/discharging rate, excellent cycling

* Corresponding authors.
E-mail addresses: zhongjin@nju.edu.cn (Z. Jin), j.liu@duke.edu (J. Liu).

http://dx.doi.org/10.1016/j.nanoen.2017.01.038
Received 21 July 2016; Received in revised form 18 October 2016; Accepted 16 January 2017
Available online 22 January 2017

stability, high reliability [27,28]. The electrode materials are the key to determine the performances of these energy devices [29–32]. Carbon based materials, especially nitrogen-doped carbon materials have shown great potential for the applications in supercapacitors and ORR (for fuel cells) [33,34], due to their high energy capacity or catalytic activity, good electrical conductivity and long cycling life. In recent years, porous carbon materials derived from naturally abundant biomass have become a class of very attractive electrode materials with remarkable performances and low cost for supercapacitors and ORR [35–39].

Nevertheless, so far very little effort has been made towards the recycling and utilization of airborne $PM_{2.5}$ for the benefit of mankind and environment. Considering the compositions of $PM_{2.5}$ aerosol are mainly elemental carbon, organic carbon and inorganic salts (such as sulfides, nitrates and ammonium salts) [40,41], it is possible to make use of the components collected from $PM_{2.5}$ after appropriate purification and treatments for positive and rewarding applications in clean energy or other fields. Of particular note, the $PM_{2.5}$ exhausts from diesel engines, as one of the main sources of global black carbon emissions [42], are dominantly consisted of carbon soot particles with diameter less than 100 nm and agglomerate chain structures of carbon soot particles with larger size [43–45]. It is very interesting and meaningful to know if these carbon soot particles can be employed for clean energy applications, rather than just contaminating the atmosphere. Here we report that the $PM_{2.5}$ derived carbon nanoparticles (termed as PM-CNPs) obtained from diesel engine emissions after thermal annealing and further purification can serve as high-performance electrode materials for supercapacitors and electrocatalytic ORR. The as-prepared PM-CNPs are doped by nitrogen element (~1.1% of atomic ratio), and with an average diameter of ~30 nm, an average pore size of ~3.3 nm. The supercapacitors based on PM-CNPs exhibit excellent specific capacity and superb stability over long-term cycling. When used as electrocatalyst, PM-CNPs show remarkable activity towards ORR. This study indicates that the recycling of $PM_{2.5}$ may turn hazardous carbon aerosol wastes of fossil-fuel-combustion into useful products for clean and sustainable energy applications.

2. Experimental section

2.1. Collection, annealing and purification of diesel engine generated $PM_{2.5}$

The $PM_{2.5}$ samples were generated by a diesel vehicle (King long XMQ6118Y1 Coach Bus) and collected with an Airmetrics MiniVol Portable Air Sampler or a Personal Environment Monitor (Buck Libra-plus-5 PK, as shown in the video of Supplementary Information) attached to the engine exhaust. Normally, 4–5 mg of $PM_{2.5}$ samples can be gathered from polytetrafluoroethylene (PTFE) filter membranes in air sampler after 1 h of collection. The $PM_{2.5}$ samples were annealed at 900 °C for 1 h under an Ar flow of 100 sccm, and then thoroughly washed sequentially by 5 wt% HF, 1.0 M HCl, deionized water and ethanol, and finally dried overnight at 110 °C. The total yield rate is roughly 55–70% after drying.

Supplementary material related to this article can be found online at doi:10.1016/j.nanoen.2017.01.038.

2.2. Synthesis of N-graphene

Firstly, graphite oxide (GO) was prepared by chemical oxidation of natural graphite under acidic conditions by a modified Hummer's method. Typically, 1g nature graphite (325 mesh, Alfa Aesar) was added to 50 mL concentrated H_2SO_4 under stirring. Then 6g $KMnO_4$ was slowly added at 30 °C and stirred for 1 h. The mixture was stirred at 90 °C for 30 min followed by the addition of 80 mL distilled water. Finally, 200 mL distilled water and 6 mL H_2O_2 (30%) was subsequently added and the color of the solution changed from brown to yellow. The generated GO was separated by centrifugation, washed and dried under vacuum. To obtain N-graphene, the GO powder was placed in a quartz tube furnace and heated under a mixed gas flow of high purity ammonia and Ar (NH_3:Ar=10:90) at 900 °C for 30 min, then the furnace was cooled down to room temperature in Ar flow.

2.3. Characterizations

The morphology and structure of samples were characterized by scanning electron microscopy (SEM, Hitachi S-4800) and transmission electron microscopy (TEM, JEOL JEM-2100). X-ray diffraction (XRD) spectra were obtained on a Shimadzu XRD-6000 X-ray diffractometer with a Cu Kα radiation source (λ=1.54178 Å) operating at 40 kV and 20 mA. Raman spectra were recorded on a Horiba JY LabRAM Evolution spectrometer with an excitation wavelength of 473 nm. X-ray photoelectron spectroscopy (XPS) was carried out on a PHI-5000 VersaProbe X-ray photoelectron spectrometer using Al Kα X-ray radiation. Nitrogen sorption isotherms were measured at 77 K using a Quantachrome Autosorb-IQ-2C-TCD-VP analyzer. The surface area was calculated using the Brunauer-Emmett-Teller (BET) method and the pore size distribution (PSD) was determined by the Barrett-Joyner-Halenda (BJH) model.

2.4. Fabrication and measurements of PM-CNP based supercapacitors

The electrodes were prepared by homogeneously mixing PM-CNPs, acetylene black (Aladdin Chemistry), PTFE binder (60 wt% suspension in water, Aladdin Chemistry) in ethanol with a weight ratio of 80:10:10. The slurry was then smeared onto a piece of nickel foam as current collector and dried in vacuum at 80 °C for 12 h. The electrochemical measurements were performed with a two-electrode system by using two comparable symmetric electrodes with about 2.0 mg of active material, an aqueous solution of 6.0 M KOH as electrolyte, and a porous cellulose separator for electrical isolation. The supercapacitor tests were also performed with a standard three-electrode system in 6.0 M KOH aqueous solution using Pt wire as counter electrode and Hg/HgO electrode as reference electrode. The working electrode was prepared with the same procedure as described above.

The cyclic voltammetry (CV), electrochemical impedance spectroscopy (EIS) and galvanostatic charge/discharge curves were recorded with a ChenHua CHI-760E electrochemical workstation. The EIS was performed with AC voltage amplitude of 5 mV in a frequency range from 0.01 to 100 kHz. The specific capacitance (C_s, F/g) of a single electrode was calculated according to the following Eq. (1):

$$C_s=\frac{2\times I\times \Delta t}{m\times \Delta V} \quad (1)$$

where I is the discharge current, m is the weight of active material in a single electrode, Δt is the discharge time and ΔV is the potential drop during discharging, respectively.

2.5. Electrocatalytic measurements of PM-CNPs towards oxygen reduction reaction

For the tests of ORR performance, CV, rotating disk electrode (RDE) voltammetry and rotating ring-disk electrode (RRDE) voltammetry were carried out at 25 °C with a ChenHua CHI-760E workstation and a Model RRDE-3A Apparatus (ALS, Japan). Ag/AgCl (with 3.0 M KCl) electrode and platinum wire were used as reference electrode and counter electrode, respectively. The catalyst ink was prepared by adding 2.0 mg of PM-CNPs into a mixture of 0.70 mL of water, 0.30 mL of ethanol, and 20 μL of Nafion (Dupont, 5 wt%) and following by ultrasonication for 1 h. Then, 10 μL of fresh catalyst ink was dropped onto a glassy carbon (GC) electrode (5 mm diameter) and dried at room temperature for 12 h in air. The CV, RDE, and RRDE

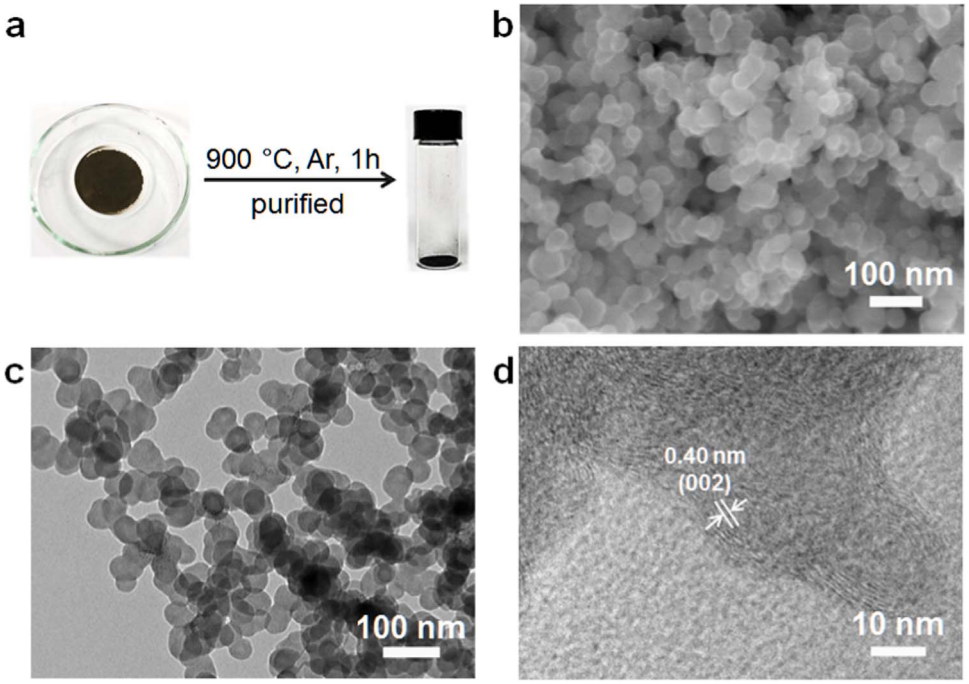

Fig. 1. (a) Optical images of the $PM_{2.5}$ sample collected by PTFE filter membrane in air sampler and the product of PM-CNPs after thermal annealing and purification. (b) SEM image, (c) TEM image, and (d) HRTEM image of as-obtained PM-CNPs.

curves were recorded in O_2-saturated 0.10 M KOH solution, and the Pt ring electrode was polarized at 0.5 V *vs.* Ag/AgCl. The electron transfer number (n) was calculated by $n=4I_{disk}/(I_{disk}+I_{ring}/N)$, where I_{disk} and I_{ring} were the disk electrode current and ring electrode current, respectively, and N was the collection efficiency of ring electrode (N=0.424). The chronoamperometric responses were tested at the bias potential of −0.2 V for 2000 s in the O_2-saturated electrolyte by constantly bubbling oxygen of 30 sccm and magnetically stirring during the whole process. In the methanol crossover tests, 1.5 mL methanol was introduced into the O_2-saturated electrolyte at 1200 s.

3. Results and discussion

3.1. Structural characterizations of PM-CNPs

The synthesis of PM-CNPs was achieved by a facile and effective "collection-annealing-purification" approach made use of diesel engine generated $PM_{2.5}$ without additional activation process. The methods of sample preparation and characterizations are detailed in the Experimental Section. Fig. 1a shows an optical image of $PM_{2.5}$ sample collected by a polytetrafluoroethylene (PTFE) filter membrane in an air sampler. The PM-CNPs were treated by thermal annealing at 900 °C in Ar flow and following washing-purification. The morphology and structural features of PM-CNPs were characterized by scanning electron microscopy (SEM) and transmission electron microscope (TEM), as shown in Fig. 1b-d. The morphologic observations reveal that the PM-CNPs consist of carbon nanoparticles with the diameter distributed between 25 and 40 nm, forming necklace-like networks (Fig. 1b and c). The PM-CNPs aggregated into a three-dimensional conductive framework with continuous particle-particle connections, which offer low electric resistance and also provides short ion transport distance, thus beneficial to improve the performances during electrochemical measurements. The high-resolution TEM image (Fig. 1d) shows that the PM-CNPs possess partially-graphitic atomic structures. The interplanar spacings of lattice fringes are approximately 0.40 nm, which is larger than the d-spacing of the (002) crystal plane of bulk graphite, which is helpful to the ion diffusion.

Powder X-ray diffraction (XRD) analysis was employed to investigate the crystalline phase of the PM-CNPs. As shown in Fig. 2a, the XRD pattern possesses a sharp peak around 25° and another weak peak around 44°, which are characteristic reflections of the (002) and (100) planes of carbon materials, respectively, consistent with the TEM results. The Raman spectrum of PM-CNPs is illustrated in Fig. 2b, showing the D band at 1358 cm^{-1} (related to defects) and the G band at 1693 cm^{-1} (related to the crystalline graphite) [46]. The peak intensity ratio of the D to G band (I_D/I_G) is about 0.94, implying the partial graphitization of PM-CNPs.

It has been reported that the compositions of diesel engine generated $PM_{2.5}$ contain carbon nanoparticles, organic species (such as long-chain alkanes and polycyclic aromatic hydrocarbons) and inorganic species (such as SO_4^{2-}, NO_3^- and NH_4^+) [39,40]. After annealing and purification, the remained components are mainly carbon and a small amount of oxygen and nitrogen (as surface species or doping elements). The chemical states and atomic ratios of C, O and N elements existed in the PM-CNPs were analyzed by XPS (Fig. S1), and the corresponding element contents are listed in Table S1. Fig. 2c shows that the C 1s signal comprises four major peaks at 284.6, 286.1, 287.8 and 289.1 eV, corresponding to C–C, C–O, C=O, and O–C=O bonds, respectively. The total N content in PM-CNPs was measured to be 1.1 at%, and the N 1s spectrum in Fig. 2d can be deconvoluted into two peaks: pyrrolic nitrogen at 400.5 eV and pyridinic nitrogen at 398.7 eV, respectively [47]. The doping of N species in the carbon frameworks may induce more electroactive sites and further improve the electrochemical performances.

To investigated the porosity of as-obtained PM-CNPs, N_2 adsorption-desorption isothermal analysis was performed. As shown in Fig. 2e, the PM-CNPs exhibits a typical type-IV N_2-isotherm with a clear hysteresis loop appearing at a wide relative pressure range (0.8–1.0 P/P_0), implying the existence of a large amount of mesopores. According to the Brunauer-Emmett-Teller (BET) method, the specific surface area of PM-CNPs was found to be 237.86 m^2/g, which is larger than multi-walled carbon nanotubes [48]. The pore size distribution of PM-CNPs was calculated using the Barrett-Joyner-Halenda (BJH) model according to the N_2 desorption isotherm part, as shown in Fig. 2f. There is a sharp peak centered at ~3.3 nm in the pore size distribution plot of the PM-CNPs, implying the existence of mesopores.

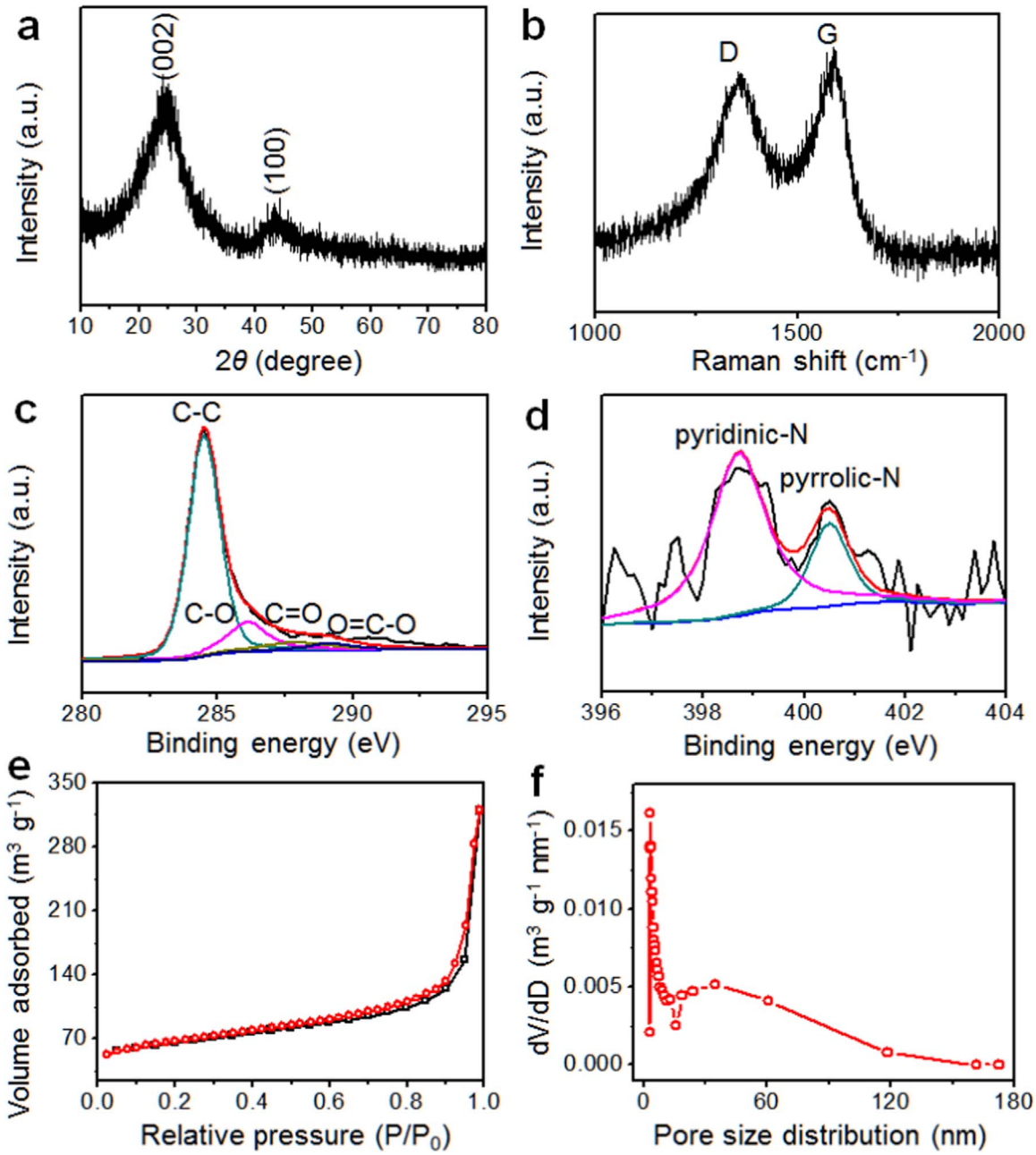

Fig. 2. (a) XRD patterns and (b) Raman spectra of as-prepared PM-CNPs. High-resolution XPS spectra of PM-CNPs at (c) C 1s and (d) N 1s regions. (e) Nitrogen adsorption-desorption isotherms and (f) BJH desorption pore-size distribution of PM-CNPs.

Besides, a broad pore distribution within 15–160 nm was also revealed. As control experiments, the PM-CNPs were also treated by thermal annealing at 800 °C or 1000 °C (termed as PM-CNPs-800 or PM-CNPs-1000, respectively) instead of 900 °C. The N_2 adsorption-desorption isotherms and pore size distribution of PM-CNPs-800 and PM-CNPs-1000 control samples (Fig. S2) are similar to the sample annealed at 900 °C. However, the specific surface area of the PM-CNPs-800 and PM-CNPs-1000 are 178.08 m^2/g and 125.74 m^2/g, respectively, lower than that of the PM-CNPs. The high surface area and large content of mesopores are crucial to the electric double-layer capacity and electrocatalytic behavior. Therefore, 900 °C is an appropriate annealing temperature for the treatment of PM-CNPs.

3.2. Electrochemical performance of PM-CNP based supercapacitors

The PM-CNPs with unique structure and special compositions were expected to act as good electrode materials for supercapacitors. Fig. 3 shows the supercapacitive performance of PM-CNPs in a two-electrode coin-type symmetric supercapacitor tested in 6 M KOH electrolyte. As shown in Fig. 3a, the cyclic voltammetry curves of PM-CNP based electrode were measured within an electrochemical window ranging from 0 to 1.0 V at scan rates of 10, 30, 50, 70 and 100 mV/s, respectively. All the CV curves show a rectangular shape. Even at the high scan rate of 100 mV/s, it maintains an approximate rectangular shape with only a little distortion, indicating the good electrochemical performance of PM-CNPs. Fig. 3b shows the galvanostatic charge/discharge curves at different current densities ranged from 0.1 to 2.0 A/g. The symmetrical shapes of the charge/discharge curves revealed the prefect reversibility of PM-CNP based electrode for charge storage and delivery at the electrode-electrolyte interfaces [49]. In addition, a negligible *IR* drop was observed at the beginning of discharge, reflecting a very small internal resistance owing to the

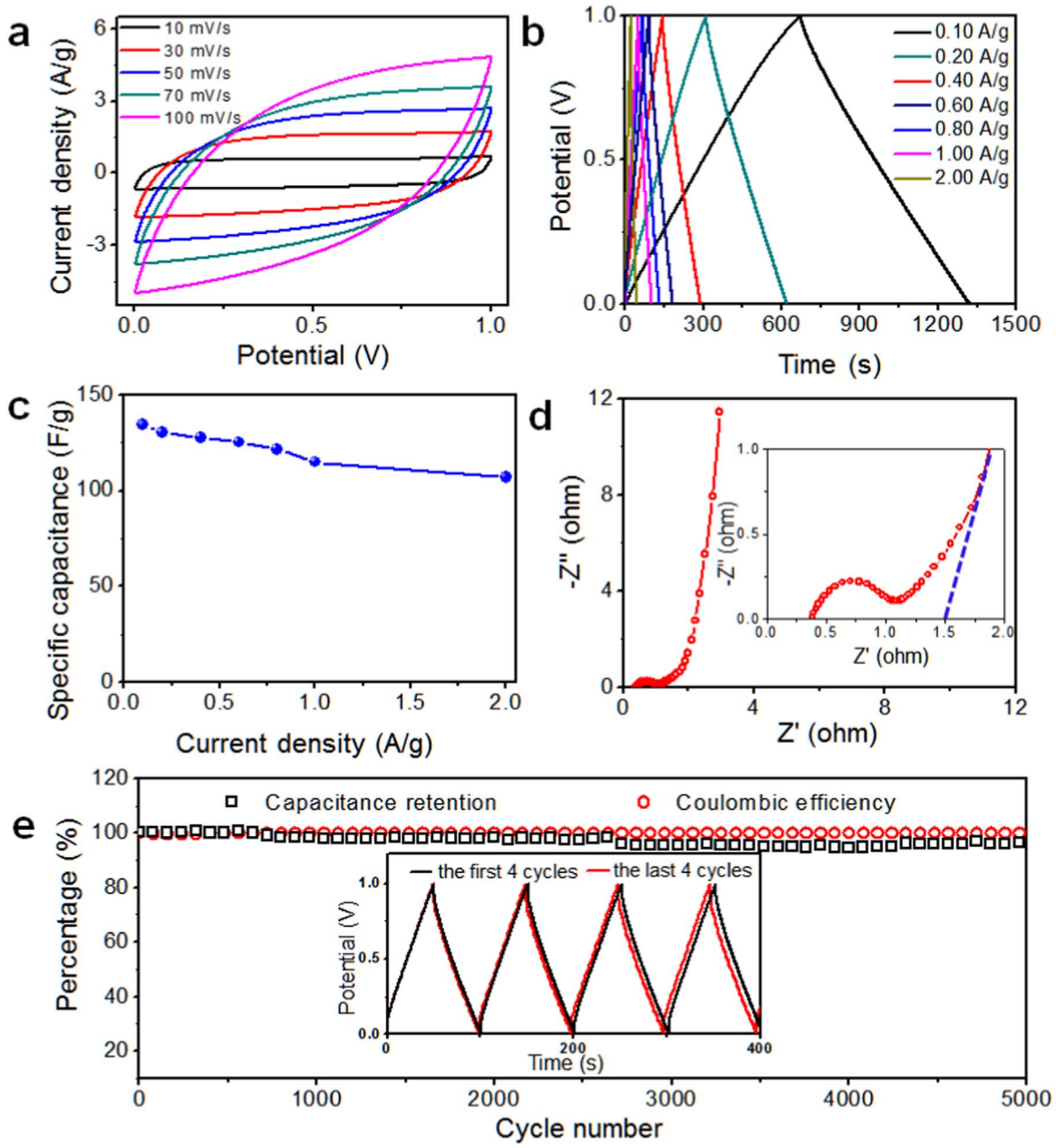

Fig. 3. Capacitive performance of PM-CNP based supercapacitors in the electrolyte of 6.0 M KOH. (a) CV curves of PM-CNP based electrode at various scan rates. (b) Charge-discharge profiles and (c) specific capacitances of PM-CNP based electrode at different current intensities. (d) Nyquist plots of PM-CNP based electrode, the details in high frequency region are shown in the insert. (e) Cycling stability and Coulombic efficiency of PM-CNP based supercapacitor at a current density of 1.0 A/g for 5000 cycles, the charge-discharge curves of the first four cycles (black line) and the last four cycles (red line) are shown in the insert.

presence of the three-dimensional conductive framework and mesopores, which may contribute to the ion transport [50]. Rate capability of the PM-CNP based electrode is depicted in Fig. 3c, the specific capacitance at 0.10 A/g is 134.4 F/g, and it remains 79.4% of this value (106.7 F/g) at a current density of 2.0 A/g. Such an excellent performance is comparable with or better than other typical carbon based materials in aqueous electrolyte, as shown in Table S2 [33,51–63]. The electrochemical capacitive performance of PM-CNPs was also measured by using a three-electrode system in electrolyte of 6.0 M KOH. Fig. S3 shows the CV curves of PM-CNP based electrode at scan rates from 5 to 70 mV/s. Clearly, the redox current increases at around −0.5 V in the CV curves, which can be ascribed to the electrochemically-active functional groups, such as pyridine-N, and pyrrolic-N groups. These nitrogen groups can induce pseudocapacitance and increase the electroactive surface area [64,65]. Due to the pseudocapacitive behavior of these electrochemically-active functional groups in PM-CNPs, the galvanostatic charge–discharge curves are not very symmetrical but distorted, which is consistent with the CV curves.

To further understand the capacitive behaviors of the PM-CNP based electrode, electrochemical impedance spectroscopic (EIS) analysis was carried out over a frequency range from 0.01 to 100 kHz. As clearly shown in Fig. 3d, Nyquist plot of the sample shows short x-intercepts, small-diameter semicircle in the high frequency region and nearly vertical slope in the low frequency region, displaying low internal resistance, low charge-transfer resistance and efficient ions diffusion. The nearly vertical line in the low frequency region of Nyquist plot indicates an ideal capacitive behavior. A resistance of 1.5 Ω was identified by extrapolating the vertical portion of the Nyquist plot to the horizontal axis, confirming a low equivalent series resistance (ESR) value of the PM-CNP based supercapacitor [66,67], consistent

well with the galvanostatic charge/discharge results (as shown in the insert in Fig. 3d).

The cycling stability is also an important factor in determining the electrode materials for many practical applications. Fig. 3e represents the cycle performance of PM-CNPs during the galvanostatic charge-discharge cycling at a current density of 1.0 A/g. During the entire process of 5000 cycles, the specific capacitance is almost constant (with a final capacitance retention of ~96%) and the Coulombic efficiency is close to 100%, indicating remarkable cycling performance. The nearly identical behaviors between the charging-discharging curves of the first four cycles and the last four cycles (as shown in the insert of Fig. 3e) further confirmed the excellent electrochemical stability. In view of the ultrahigh specific capacitance and cycle stability of PM-CNP based electrode, we hope these results will bring inspiration to environmental protection and resource recycling.

3.3. Electrocatalytic performance of PM-CNPs towards oxygen reduction reaction

Beside the capacitive behavior, the porosity and nitrogen-doping of PM-CNPs are also valuable for electrocatalytic applications. In order to evaluate the electrocatalytic ORR performance, cyclic voltammetry (CV), rotating disk electrode (RDE), rotating ring disk electrode (RRDE), and methanol crossover measurements of PM-CNPs were performed in alkaline medium, as plotted in Fig. 4. For comparison, we also prepared nitrogen-doped graphene (N-graphene, as detailed in the Section 2) as a control sample and tested its ORR activities. Based on XPS analysis, the total N content in N-graphene was measured to be 3.64%, similar with the previous report [68]. The total surface area of N-graphene was measured to be 185.69 m^2/g through BET method, which is smaller than that of PM-CNPs. The Raman spectrum of N-graphene is also shown in Fig. S4. The characteristic peaks of N-graphene are located around 1601 cm^{-1} (G band) and 1357 cm^{-1} (D band). The CV curves of PM-CNPs and N-graphene in O_2-saturated 0.1 M KOH solution are shown in Fig. 4a. It can be seen that the onset and reduction peak potentials of PM-CNPs are at −0.066 V and −0.217 V, whereas those for N-graphene are at −0.107 V and −0.254 V, respectively. Compared with N-graphene and other N-doped carbon catalysts in previous reports (Table S3) [69–74], the onset potential of PM-CNPs is higher than that of N-graphene, CMTs-750 [69], NG [70], g-C_3N_4/C [72], 950-G1AG1 [73] and $NCNC_{900}$ [74], indicating PM-CNPs is a promising N-doped carbon catalyst for ORR. To further investigate the kinetics for ORR, linear sweep voltammetry (LSV) measurements were carried out at various rotation speeds (400–2500 rpm) (Fig. 4b). The electrocatalytic activity of these two metal-free electrocatalysts was further evaluated by RDE voltammetry and compared with commercially-available Pt/C catalyst (20 wt%, Johnson Matthey). As shown in Fig. 4b, the onset potential of the PM-CNPs is −0.065 V, which is higher than that of the N-graphene (−0.112 V) and consistent well with the CV results. Though the onset potential of the PM-CNPs is lower than that of the Pt/C catalyst (−0.005 V), the limiting current density is close to that of the Pt/C catalyst. The transferred electron number (n) during the ORR process can be calculated from RRDE voltammogram (Fig. 4c). As shown in Fig. S5, the n values of PM-CNPs and N-graphene based electrode are calculated to be 3.5 and 2.6 when the disk electrode current (I_{disk}) has reached a relative stable value around −0.80 V. This result suggests that PM-CNP based electrode has a higher selectivity to reduce O_2 to H_2O than that of N-graphene. Moreover, the PM-CNPs, N-graphene control sample and commercially-available Pt/C catalyst were further evaluated by the test of methanol crossover. After the introduction of 1.5 mL methanol, the ORR current of PM-CNP based electrode only

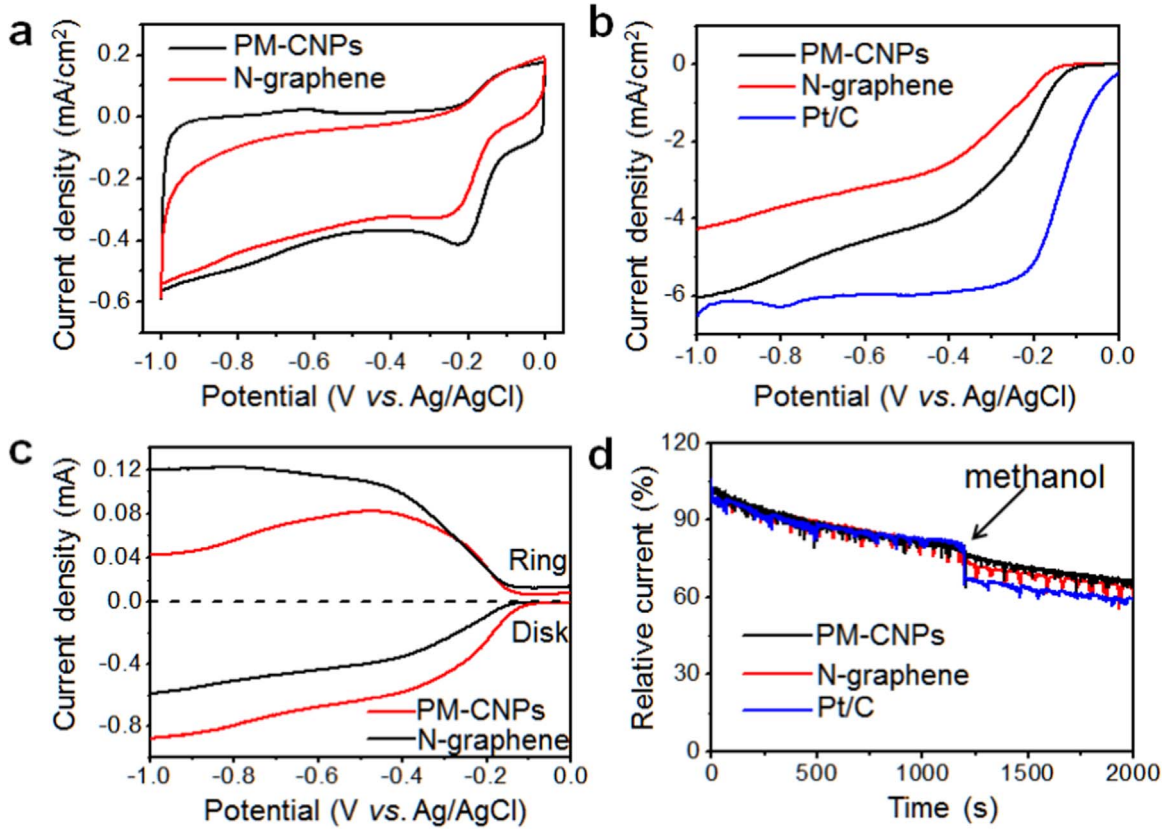

Fig. 4. Electrocatalytic performance of PM-CNP based electrode towards ORR. (a) CV curves of PM-CNPs and N-graphene (control sample) at a scan rate of 50 mV/s in O_2-saturated 0.10 M KOH electrolyte. (b) LSV curves of PM-CNPs, N-graphene and commercially-available Pt/C catalyst measured by RDE at a scan rate of 10 mV/s and rotation speed of 2500 rpm. (c) RRDE measurements of PM-CNPs and N-graphene at a rotation rate of 2500 rpm with the Pt ring electrode polarized at 0.50 V. (d) Chronoamperometric responses of PM-CNPs, N-graphene and Pt/C catalyst in the O_2-saturated electrolyte by introducing 1.5 mL of methanol into the electrolyte at the time of 1200 s.

slightly reduced; the relative current decrease of N-graphene was larger than that of PM-CNPs, while that of Pt/C catalyst suffered a sharp decrease (Fig. 4d). The better resistance of PM-CNPs against methanol may be ascribed to the lower methanol wettability. Fig. S6 shows the methanol contact angle measurements of PM-CNPs and N-graphene. The methanol contact angle of PM-CNPs is ~28.9°, which is higher than that of N-graphene (7.8°). The result indicates that PM-CNPs possess better immunity towards methanol crossover. The good ORR activity and high stability towards methanol crossover of as-prepared PM-CNPs indicates the great potential in advanced electrocatalysts.

4. Conclusion

In summary, for the first time, we found that the mesoporous and nitrogen-doped carbon nanoparticles derived from diesel engine $PM_{2.5}$ emissions can serve as excellent electrode material for supercapacitors and efficient metal-free electrocatalysts towards ORR. By the facile "collection-annealing-purification" approach, $PM_{2.5}$, which may cause serve harms to human health and atmospheric environment, has been turned into useful substance. The as-obtained PM-CNPs could be employed as electrode material in energy conversion and storage field with the following highlighted features: (1) the nitrogen-doped PM-CNPs possess the advantages of large specific surface area, porous structure, and good conductivity. (2) The PM-CNP based supercapacitors exhibit excellent specific capacity and superb stability over long-term cycling. Notably, the PM-CNP based supercapacitors display remarkable charge storage capacity with a specific capacitance of 134.4 F/g in 6.0 M KOH at a current density of 0.1 A/g and good stability over 5000 cycles. (3) The PM-CNPs also show good ORR electrocatalytic activity and better stability towards methanol crossover than that of commercially-available Pt/C catalyst.

Overall, these results reveal the development of a simple and effective strategy for the recycling of high-performance carbon material from $PM_{2.5}$ aerosol. Together with high porosity, electrochemical activity and stability, the PM-CNPs provide us a novel electrode material with great potential in energy conversion and storage. Moreover, the utilization of carbonaceous waste materials recycled from PM pollution could provide new inspiration for air pollution control and circular economy. We expect that this work will raise more attention and efforts for the reduction of environmental pollution by turning harmful wastes into useful products and promoting the developments of sustainable clean energy.

Acknowledgements

This work is supported by the National Thousand Young Talents Program of China, the Young Scientists Project of National Basic Research Program of China (973 Program No. 2015CB659300), the National Natural Science Foundation of China (No. 21403105 and 21573108), the China Postdoctoral Science Foundation (No. 2015M580408, 2015M581775, 2015M580413 and 2015M581769), the Natural Science Foundation for Young Scholars of Jiangsu Province (No. BK20150583, BK20150571, BK20160643 and BK20160647), the Fundamental Research Funds for the Central Universities and a project funded by the Priority Academic Program Development (PAPD) of Jiangsu Higher Education Institutions.

Appendix A. Supporting information

Supplementary data associated with this article can be found in the online version at doi:10.1016/j.nanoen.2017.01.038.

References

[1] P. Simon, Y. Gogotsi, Nat. Mater. 7 (2008) 845–854.
[2] J. Yan, Q. Wang, T. Wei, Z. Fan, Adv. Energy Mater. 4 (2014) 1300816.
[3] R. Zhang, J. Jing, J. Tao, S.C. Hsu, G. Wang, J. Cao, C.S. Lee, L. Zhu, Z. Chen, Y. Zhao, Z. Shen, Atmos. Chem. Phys. 13 (2013) 7053–7074.
[4] S. Pateraki, D.N. Asimakopoulos, T. Maggos, C. Vasilakos, J. Hazard. Mater. 182 (2010) 801–811.
[5] A. Nel, Science 308 (2005) 804–806.
[6] N. Mahowald, Science 334 (2011) 794–796.
[7] D.E. Horton, C.B. Skinner, D. Singh, N.S. Diffenbaugh, Nat. Clim. Change 4 (2014) 698–703.
[8] L.P. Naeher, K.R. Smith, B.P. Leaderer, L. Neufeld, D.T. Mage, Environ. Sci. Technol. 35 (2001) 575–581.
[9] C.A. Pope, D.W. Dockery, J. Air Waste Manag. Assoc. 56 (2006) 709–742.
[10] S.C. Anenberg, L.W. Horowitz, D.Q. Tong, J.J. West, Environ. Health Perspect. 118 (2010) 1189–1195.
[11] K.L. Timonen, E. Vanninen, J.D. Hartog, A. Ibald-Mulli, B. Brunekreef, D.R. Gold, J. Heinrich, G. Hoek, T. Lanki, A. Peters, T. Tarkiainen, P. Tiittanen, W. Kreyling, J. Pekkanen, J. Expo. Sci. Environ. Epidemiol. 16 (2006) 332–341.
[12] J.C. Chow, J.G. Watson, Energy Fuels 16 (2002) 222–260.
[13] C.M. Somers, B.E. McCarry, F. Malek, J.S. Quinn, Science 304 (2004) 1008–1010.
[14] S.M. Platt, I.E. Haddad, S.M. Pieber, R.J. Huang, A.A. Zardini, M. Clairotte, R. Suarez-Bertoa, P. Barmet, L. Pfaffenberger, R. Wolf, J.G. Slowik, S.J. Fuller, M. Kalberer, R. Chirico1, J. Dommen, C. Astorga, R. Zimmermann, N. Marchand, S. Hellebust, B. Temime-Roussel, U. Baltensperger, A.S.H. Prévôt, Nat. Commun. 5 (2014) 3749.
[15] C.B. Han, T. Jiang, C. Zhang, X. Li, C. Zhang, X. Cao, Z.L. Wang, ACS Nano 9 (2015) 12552–12561.
[16] C. Liu, P.C. Hsu, H.W. Lee, M. Ye, G. Zheng, N. Liu, W. Li, Y. Cui, Nat. Commun. 6 (2015) 6205.
[17] B.C.H. Steele, A. Heinzel, Nature 414 (2001) 345–352.
[18] J.K. Nørskov, J. Rossmeisl, A. Logadottir, L. Lindqvist, J. Phys. Chem. B 108 (2004) 17886–17892.
[19] T. Hyeon, S. Han, Y.E. Sung, K.W. Park, Y.W. Kim, Angew. Chem. 115 (2003) 4488–4492.
[20] C. Liu, Z. Yu, D. Neff, A. Zhamu, B.Z. Jang, Nano Lett. 10 (2010) 4863–4868.
[21] Y. Zhu, S. Murali, M.D. Stoller, K.J. Ganesh, W.W. Cai, P.J. Ferreira, A. Pirkle, R.M. Wallace, K.A. Cychosz, M. Thommes, D. Su, E.A. Stach, R.S. Ruoff, Science 332 (2011) 1537–1541.
[22] L.L. Zhang, X.S. Zhao, Chem. Soc. Rev. 38 (2009) 2520–2531.
[23] L.F. Cui, Y. Yang, C.M. Hsu, Y. Cui, Nano Lett. 9 (2009) 3370–3374.
[24] H. Li, Z. Wang, L. Chen, X. Huang, Adv. Mater. 21 (2009) 4593–4607.
[25] P. Poizot, S. Laruelle, S. Grugeo, L. Dupont, J.M. Tarascon, Nature 407 (2000) 496–499.
[26] M.K. Debe, Nature 486 (2012) 43–51.
[27] Y. Wang, Z. Shi, Y. Huang, Y. Ma, C. Wang, M. Chen, Y. Chen, J. Phys. Chem. C 113 (2009) 13103–13107.
[28] H.P. Cong, X.C. Ren, P. Wang, S.H. Yu, Energy Environ. Sci. 6 (2013) 1185–1191.
[29] X. Lang, A. Hirata, T. Fujita, M. Chen, Nat. Nanotech. 6 (2011) 232–236.
[30] Y. Liang, Y. Li, H. Wang, J. Zhou, J. Wang, T. Regier, H. Dai, Nat. Mater. 10 (2011) 780–786.
[31] H. Wang, Y. Liang, Y. Li, H. Dai, Angew. Chem. Int. Ed. 50 (2011) 10969–10972.
[32] J. Xiao, L. Wan, S. Yang, F. Xiao, S. Wang, Nano Lett. 14 (2014) 831–838.
[33] T. Lin, I.W. Chen, F. Liu, C. Yang, H. Bi, F. Xu, F. Huang, Science 350 (2015) 1508–1513.
[34] K. Gong, F. Du, Z. Xia, M. Durstock, L. Dai, Science 323 (2009) 760–764.
[35] K. Jurewicz, K. Babel, Energy Fuels 24 (2010) 3429–3435.
[36] Y. Li, G. Wang, T. Wei, Z. Fan, P. Yan, Nano Energy 19 (2016) 165–175.
[37] T. Yang, T. Qian, M. Wang, X. Shen, N. Xu, Z. Sun, C. Yan, Adv. Mater. 28 (2016) 539–545.
[38] C. Guo, W. Liao, Z. Li, L. Sun, C. Chen, Nanoscale 7 (2015) 15990–15998.
[39] J. Zhang, Y. Cai, Q. Zhong, D. Lai, J. Yao, Nanoscale 7 (2015) 17791–17797.
[40] H. Wang, Y. Zhuang, Y. Wang, Y. Sun, H. Yuan, G. Zhuang, Z. Hao, China, J. Environ. Sci. China 20 (2008) 1323–1327.
[41] X.L. Han, L.P. Naeher, Environ. Int. 32 (2006) 106–120.
[42] T.C. Bond, S.J. Doherty, D.W. Fahey, P.M. Forster, T. Berntsen, B.J. DeAngelo, M.G. Flanner, S. Ghan, B. Kärcher, D. Koch, S. Kinne, Y. Kondo, P.K. Quinn, M.C. Sarofim, M.G. Schultz, M. Schulz, C. Venkataraman, H. Zhang, S. Zhang, N. Bellouin, S.K. Guttikunda, P.K. Hopke, M.Z. Jacobson, J.W. Kaiser, Z. Klimont, U. Lohmann, J.P. Schwarz, D. Shindell, T. Storelvmo, S.G. Warren, C.S. Zender, J. Geophys. Res.: Atmos. 118 (2013) 5380–5552.
[43] D.B. Kittelson, M. Arnold, W.F. Watts, Review of diesel particulate matter sampling methods, Final Report. Minneapolis, 1999.
[44] H. Burtscher, J. Aerosol Sci. 3 (2005) 896–932.
[45] Z. Ning, K.L. Chan, K.C. Wong, D. Westerdahl, G. Močnik, J.H. Zhoue, C.S. Cheunge, Atmos. Environ. 80 (2013) 31–40.
[46] M. Sevilla, A.B. Fuertes, ACS Nano 8 (2014) 5069–5078.
[47] J. Hou, C. Cao, F. Idrees, X. Ma, ACS Nano 9 (2015) 2556–2564.
[48] B.J. Yoon, S.H. Jeong, K.H. Lee, H.S. Kim, C.G. Park, J.H. Han, Chem. Phys. Lett. 388 (2004) 170–174.
[49] L. Deng, R.J. Young, I.A. Kinloch, A.M. Abdelkader, S.M. Holmes, D.A. De Haro-Del Rio, S.J. Eichhorn, ACS Appl. Mater. Interfaces 5 (2013) 9983–9990.
[50] D.W. Wang, F. Li, M. Liu, G.Q. Liu, H.M. Cheng, Angew. Chem. 120 (2008) 379–382.
[51] C.G. Liu, M. Liu, F. Li, H.M. Cheng, Appl. Phys. Lett. 92 (2008) 143108.
[52] C. Yu, C. Masarapu, J. Rong, B. Wei, H. Jiang, Adv. Mater. 21 (2009) 4793–4797.
[53] A. Yu, I. Roes, A. Davies, Z. Chen, Appl. Phys. Lett. 96 (2010) 253105.
[54] J. Yan, Z. Fan, T. Wei, W. Qian, M. Zhang, F. Wei, Carbon 48 (2010) 3825–3833.
[55] J. Yan, T. Wei, B. Shao, F. Ma, Z. Fan, M. Zhang, C. Zheng, Y. Shang, W. Qian,

F. Wei, Carbon 48 (2010) 1731–1737.
[56] M. Genovese, J. Jiang, K. Lian, N. Holm, J. Mater. Chem. A 3 (2015) 2903–2913.
[57] A.R. John, P. Arumugam, J. Power Sources 277 (2015) 387–392.
[58] N. Jäckel, D. Weingarth, M. Zeiger, M. Aslan, I. Grobelsek, V. Presser, J. Power Sources 272 (2014) 1122–1133.
[59] Y. Liu, J. Zhou, L. Chen, P. Zhang, W. Fu, H. Zhao, Y. Ma, X. Pan, Z. Zhang, W. Han, E. Xie, ACS Appl. Mater. Interfaces 7 (2015) 23515–23520.
[60] S. Zheng, H. Ju, X. Lu, Adv. Energy Mater. 5 (2015) 1500871.
[61] H. Wang, L. Zhi, K. Liu, K. Liu, L. Dang, Z. Liu, Z. Lei, C. Yu, J. Qiu, Adv. Funct. Mater. 25 (2015) 5420–5427.
[62] J. Zhu, J. Yang, R. Miao, Z. Yao, X. Zhuang, X. Feng, J. Mater. Chem. A4 (2016) 2286–2292.
[63] K. Yuan, Y. Xu, J. Uihlein, G. Brunklaus, L. Shi, R. Heiderhoff, M. Que, M. Forster, T. Chassé, T. Pichler, T. Riedl, Y. Chen, U. Scherfet, Adv. Mater. 27 (2015) 6714–6721.
[64] D. Hulicova-Jurcakova, M. Kodama, H. Hatori, Chem. Mater. 18 (2006) 2318–2326.
[65] D. Hulicova-Jurcakova, M. Kodama, S. Shiraishi, H. Hatori, Z.H. Zhu, G.Q. Lu, Adv. Funct. Mater. 19 (2009) 1800–1809.
[66] Y. Xu, Z. Lin, X. Zhong, X. Huang, N.O. Weiss, Y. Huang, X. Duan, Nat. Commun. 5 (2014) 4554.
[67] T.Y. Kim, G. Jung, S. Yoo, K.S. Suh, R.S. Ruoff, ACS Nano 7 (2013) 6899–6905.
[68] X. Li, H. Wang, J.T. Robinson, H. Sanchez, G. Diankov, H. Dai, J. Am. Chem. Soc. 131 (2009) 15939–15944.
[69] Y. Ma, J. Zhao, L. Zhang, Y. Zhao, Q. Fan, X. Li, Z. Hu, W. Huang, Carbon 49 (2011) 5292–5297.
[70] Z. Lin, G. Waller, Y. Liu, M. Liu, C.P. Wong, Adv. Energy Mater. 2 (2012) 884–888.
[71] S. Yang, L. Zhi, K. Tang, X. Feng, J. Maier, K. Mullen, Adv. Funct. Mater. 22 (2012) 3634–3640.
[72] J. Liang, Y. Zheng, J. Chen, J. Liu, D. Hulicova-Jurcakova, M. Jaroniec, S.Z. Qiao, Angew. Chem. Int. Ed. 51 (2012) 3892–3896.
[73] N. Brun, S.A. Wohlgemuth, P. Osiceanu, M.M. Titirici, Green Chem. 15 (2013) 2514–2524.
[74] S. Shanmugam, T. Osaka, Chem. Commun. 47 (2011) 4463–4465.

Guoyin Zhu obtained his M.S. degree from Nanjing University of Posts & Telecommunications in 2014. Currently, he is pursuing his Ph.D. degree under the supervision of Prof. Zhong Jin and Jie Liu at Nanjing University. His research is mainly focused on the synthesis of carbonaceous nanomaterials, and their application for energy conversion and storage devices.

Dr. Tao Chen received his Ph.D. degree in Chemical Engineering and Technology under supervision of Prof. Jiajun Fu from Nanjing University of Science and Technology in June 2015. He is currently a postdoctoral researcher in the group of Prof. Zhong Jin at Nanjing University. His current research focuses on the design and synthesis of nanostructured electrode materials for sodium and lithium ion batteries.

Yi Hu received his B.S. degree in Chemistry from Sichuan University in 2014. He is now pursuing his Ph.D. degree under the supervision of Prof. Zhong Jin in School of Chemistry and Chemical Engineering at Nanjing University. His research interests reside in two-dimensional nanomaterials for electrochemical energy storage and photoelectric conversion.

Lianbo Ma received his M.S. degree in Applied Chemistry from Jiangsu University, PR China (2015). He is now pursing his Ph.D. degree under the supervision of Prof. Zhong Jin and Jie Liu in School of Chemistry and Chemical Engineering, Nanjing University, P.R. China. His main interest is the design and fabrication nanomaterials for energy storage, electrochemistry, and photoelectric conversion.

Renpeng Chen has graduated from the Northeastern University (China) since 2014. Now, he is pursuing his M.S. degree under the guidance of Prof. Zhong Jin in School of Chemistry and Chemical Engineering at Nanjing University. His research interest is focused on the synthesis of alloy materials for lithium-ion batteries.

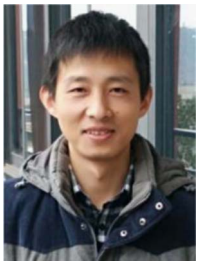

Dr. Hongling Lv received his Ph.D. degree in Materials Processing Engineering under supervision of Professor Jieming Cao from Nanjing University of Aeronautics and Astronautics (2014). He is currently a postdoctoral researcher in the group of Prof. Zhong Jin at Nanjing University. His current research activities focus on key materials for lithium–ion batteries, lithium–sulfur batteries and lithium–selenium batteries.

Yanrong Wang received her master degree in physical chemistry under the supervision of Professor Yong Hu in College of Chemistry and life sciences at Zhejiang Normal University in 2015. She is now pursuing her Ph.D. degree under the supervision of Prof. Zhong Jin and Jie Liu in School of Chemistry and Chemical Engineering at Nanjing University. Her current research interest is the design of new type of battery.

Dr. Jia Liang received his Ph.D. in the Key Laboratory for Physics and Chemistry of Nanodevices from Peking University in 2015, under the guidance of Prof. Gengmin Zhang. He joined Prof. Jun Lou's research group in Rice University as a visiting student in 2014. He is currently an assistant researcher in the group directed by Prof. Zhong Jin and Jie Liu at Nanjing University. His main research interest is synthesis of energy nanomaterials and their applications in solar cells, catalyses, and flow batteries.

Xiaojie Li entered China Pharmaceutical University in 2012. She majors in chemistry and currently works as an assistant of Dr. Changzeng Yan in the group of Prof. Zhong Jin. Her current research focuses on designing and fabrication of novel photocatalysts for solar energy conversion applications.

Dr. Changzeng Yan received his Ph.D. degree from Sungkyunkwan University in Korea in August of 2014 under the supervision of Prof. Dae Joon Kang. He is currently working as a postdoctoral research fellow in Prof. Zhong Jin's research group at School of Chemistry and Chemical Engineering, Nanjing University. His research interests include designing and fabrication of novel photocatalysts for solar energy conversion applications: water splitting, CO_2 reduction, and N_2 fixation. He aims to employ varieties of synergistic effects resulting from nano-heterostructures to enhance the energy conversion efficiency.

Dr. Hongfei Zhu received his B.S. (2001) from Huaihai Institute of Technology and Ph.D. (2011) in the Institute of chemistry, CAS. He worked as a postdoctoral scholar at Suzhou Institute of nano-tech and nano-bionics, CAS. Now he is an associate research fellow in School of Chemistry and Chemical Engineering at Nanjing University. His research interest includes: flexible electronics, 2D materials, nanomaterials based electronic devices (include photovoltaic devices, FET, photodetectors, OLEDs, etc.).

Dr. Haixia Liu received her Ph.D. degree from Xiamen University (2014), Xiamen, China. She is currently an assistant researcher in the group directed by Prof. Zhong Jin and Jie Liu at Nanjing University. Her main research interest is the synthesis of nanomaterials and their applications in photoelectrochemistry.

Dr. Zuoxiu Tie received her B.S. (2004) degree and Ph.D. (2010) from Nanjing University. She is currently a research associate in the group of Prof. Zhong Jin. Her current research interest focuses on carbonaceous nanomaterials for energy conversion and storage devices.

Prof. Zhong Jin received his B.S. (2003) and Ph.D. (2008) in chemistry from Peking University. He worked as a postdoctoral scholar at Rice University and Massachusetts Institute of Technology. Now he is a professor in School of Chemistry and Chemical Engineering at Nanjing University. He leads a research group working on advanced materials and devices for energy conversion and storage.

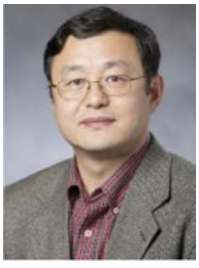

Prof. Jie Liu is currently the George B. Geller Professor of Chemistry at Duke University and an adjunct professor of "Thousands Talents" Program at Nanjing University. He earned a B.S. from Shandong University in 1987 and a Ph.D. from Harvard University in 1996. His research interests include the synthesis and chemical functionalization of nanomaterials, nanoelectronic devices, scanning probe microscopy, and carbon nanomaterials. Prof. Liu is a Fellow of the AAAS, APS and RSC.